Linear polarization of dielectronic satellite lines of hydrogenlike ions with Z values ranging from 9 to 92

Tianluo Luo,[1,*] Zhencen He,[2,1,*] Zhihao Yang,[3] Shuyu Zhang,[2] and Zhimin Hu[1,†]

[1]*Key Laboratory of Radiation Physics and Technology of Ministry of Education, Institute of Nuclear Science and Technology, Sichuan University, Chengdu 610064, China*

[2]*West China School of Basic Medical Sciences and Forensic Medicine, Sichuan University, Chengdu 610041, China*

[3]*College of Intelligent Manufacturing, Sichuan University of Arts and Science, Dazhou 635000, China*

(Received 8 November 2023; accepted 5 February 2024; published 22 February 2024)

A systematic investigation of dielectronic satellite lines in hydrogenlike ions with Z values ranging from 9 to 92 is carried out, with a focus on the effects of the Breit interaction and the generalized Breit interaction on their linear polarization. We present a detailed analysis of the polarization behaviors and resonance strengths of the satellite lines, facilitating the spectral analysis under the electron-beam ion-trap measurement conditions. Emphasizing the second-step radiative decay process in dielectronic recombination of hydrogenlike Ti^{21+}, Kr^{35+}, Mo^{41+}, and U^{91+} ions, the alignment parameters of the singly excited states are determined by using both the deorientation factor formalism and density-matrix theory. These calculations indicate a promising opportunity for understanding the effect of the Breit interaction as well as differentiating the formalism of the deorientation factor and the density-matrix theory for the calculations of dielectronic satellite lines.

DOI: 10.1103/PhysRevA.109.022815

I. INTRODUCTION

Dielectronic recombination (DR) is one of the most important electron-ion collision processes in hot plasmas. One of the distinctive features of DR is the resonance nature, resulting in a substantially larger cross section than other recombination processes. Consequently, it is important for understanding the hot plasmas, including, e.g., astrophysical plasmas [1–5] and fusion plasmas [6,7]. Dielectronic recombination can be considered as a two-step process. The first step is dielectronic capture, which is the time-reversed process of the Auger decay. The highly charged ion captures an electron and simultaneously excites an electron, and then a doubly excited state is formed. For the DR of hydrogenlike ions, the second step involves successive radiative processes. The doubly excited ions decay by sequentially emitting two x rays with similar energies, which can be expressed as

$$\begin{aligned} e + A^{q+} &\rightarrow A^{(q-1)+**} \rightarrow A^{(q-1)+*} + h\nu_1 \\ &\rightarrow A^{(q-1)+} + h\nu_2 + h\nu_1. \end{aligned} \tag{1}$$

The investigation of the angular distribution and polarization of emitted x rays plays a crucial role in the study of hot plasmas. These measurements offer unique insights into the collision dynamics of highly charged ions and the geometric information of the hot plasmas [8–27]. In recent years, due to the advance of detection technology [28–30], many measurements of the angular distribution and polarization of emitted x rays from electron-ion collisions have been studied in electron-beam ion traps (EBITs) and storage rings [8–14]. The study of relativistic effects has been an important theme, such as the spin-flip effect in radiative recombination [15–20], hyperfine interaction [21–24], and multipole mixing of radiation fields [25,26]. In particular, the Breit interaction (BI), which is the relativistic correction of the electron-electron interaction, has attracted much interest. Notably, recent measurements of the angular distribution and the integral resonant strength of the $(1s2s^22p_{1/2})_1 \rightarrow (1s^22s^2)_0$ electric dipole ($E1$) transition of lithiumlike Au^{76+} [9] confirmed the dominance of the BI on the angular distribution of the DR x rays and demonstrated a strong Z dependence. Furthermore, the investigation of the angular distribution and polarization of the satellite lines, which refer to the x-ray lines that accompany and are energy adjacent to the main x-ray lines, can provide qualitative information on the plasma state [31,32]. Indeed, the directionality of anisotropic plasma electrons not only leads to polarized x rays but also induces anisotropic x-ray emissions [33–35]. This can affect the observed intensity of x-ray satellite lines and significantly affect temperature or density diagnostics. The earliest study of relativistic effects on the angular distribution and polarization of dielectronic satellite lines of hydrogenlike ions was conducted by Chen and Scofield [33]. They carried out relativistic calculations of angular asymmetry parameters and polarization for a sequence of hydrogenlike ions with $Z = 9$, 22, 28, 42, and 92 using the multiconfiguration Dirac-Fock model. However, experimental measurements of the angular distribution and linear polarization of dielectronic satellite lines in hydrogenlike ions are still limited. Two factors might contribute to this scarcity. First is the limit of experimental facilities and detection technology. Second is the deficiency of systematic calculation concerning the linear polarization and

*These authors contributed equally to this work.
†huzhimin@scu.edu.cn

resonance strengths of dielectronic satellite lines of hydrogenlike ions.

In this paper we present the linear polarization of dielectronic satellite lines of hydrogenlike ions with Z values ranging from 9 to 92. Special attention is paid to the effects of BI and the generalized Breit interaction (GBI) on the polarization of these lines. Moreover, we propose feasible measurements of linear polarization of dielectronic satellite lines of hydrogenlike ions at EBITs. The angular distribution coefficient in the direction perpendicular to the electron-beam axis from the two-step radiative decay process is further investigated to obtain the relative intensity of the dielectronic satellite lines. The polarization of the second-step radiative decay is calculated by two methods, namely, the formalism of the deorientation factor [36] and the density-matrix method [37]. The synthetic spectra are obtained by convolving the theoretical line intensity with the experimental resolution and the natural linewidth. Finally, to propose the feasible polarization measurement of the dielectronic satellite lines of hydrogenlike ions at EBITs, the effective polarization is calculated.

II. THEORY

The partial cross section of the first-step radiative decay is conducted by using the flexible atomic code based on the configuration-interaction method [38]. Additionally, the calculation of the second-step radiative decay photons is made with the formalism of the deorientation factor [36] and the density-matrix theory [37]. Dielectronic recombination involves different transitions between four states, i.e., the initial state $|i\rangle$, the singly excited state $|s\rangle$, the doubly excited state $|d\rangle$, and the ground state $|g\rangle$, following the second-step radiative decay. Note that there is an important two-photon decay in the second-step radiative decay [39,40],

$$(1s2s)_0 \rightarrow (1s^2)_0 + h\nu_2 + h\nu_1. \tag{2}$$

Nevertheless, these two photons share the transition energy between these two states. However, their energies are relatively low and outside the photon energies investigated in the present work.

A. Alignment parameters and the Breit interaction

Using the density-matrix theory [41], the reduced amplitudes $\langle \varepsilon_d J_d || V || \varepsilon_i J_i, l\, j : J_d \rangle$ describe the formation of a doubly excited state $|d\rangle$ arising from the interaction between the bound electron of state $|i\rangle$ and the free electron $(l\, j)$. Here J_d and J_i are total angular momenta for the states $|d\rangle$ and $|i\rangle$, respectively, and ε represents all additional quantum numbers that are needed for its unique specification. Following Ref. [41], the statistical tensors of the doubly excited state $|d\rangle$ [42] can be written as

$$\rho_k^d = \frac{A}{8\pi(2J_i+1)} \sum_{ll'jj'} (-1)^{J_d+J_i-1/2} (l, l', j, j')^{1/2} \langle \varepsilon_d J_d || V || \varepsilon_i J_i, l\, j : J_d \rangle \langle \varepsilon_d J_d || V || \varepsilon_i J_i, l'\, j' : J_d \rangle^* \times \begin{Bmatrix} j & l & 1/2 \\ l' & j' & k \end{Bmatrix} \begin{Bmatrix} j & J_d & J_i \\ J_d & j' & k \end{Bmatrix} \langle l 0 l' 0 | k 0 \rangle, \tag{3}$$

where A denotes a normalization constant. When calculating the angular distribution and polarization of x rays emitted in electron-ion collisions, one usually uses the reduced statistical tensors ρ_k^d/ρ_0^d to describe the magnetic sublevel population of excited ions and atoms. The reduced statistical tensors are called alignment parameters, which can be expressed as

$$\mathcal{A}_k^d = \frac{(2J_d+1)^{1/2}}{\sum_{lj} |\langle \varepsilon_d J_d || V || \varepsilon_i J_i, l\, j : J_d \rangle|^2} \sum_{ll'jj'} (-1)^{J_d+J_i-1/2} (l, l', j, j')^{1/2} \langle \varepsilon_d J_d || V || \varepsilon_i J_i, l\, j : J_d \rangle \langle \varepsilon_d J_d || V || \varepsilon_i J_i, l'\, j' : J_d \rangle^* \times \begin{Bmatrix} j & l & 1/2 \\ l' & j' & k \end{Bmatrix} \begin{Bmatrix} j & J_d & J_i \\ J_d & j' & k \end{Bmatrix} \langle l 0 l' 0 | k 0 \rangle, \tag{4}$$

where $\langle \cdots | \cdots \rangle$ is the Clebsch-Gordan coefficient, the symbol $(a, b, \ldots)$ denotes the product $(2a+1)(2b+1)\cdots$, $\{\vdots\}$ denotes the Wigner 6-j symbols, and V is the interaction potential of N electrons, which can be expressed as

$$V = \sum_{i<j}^{N} \left(V_{ij}^C + V_{ij}^B \right). \tag{5}$$

The first term is the Coulomb interaction

$$V_{ij}^C = \frac{1}{r_{ij}} \tag{6}$$

and the second term is GBI which contains two parts, i.e., the magnetic interaction

$$V_{ij}^{\mathrm{mag}} = -(\boldsymbol{\alpha_i} \cdot \boldsymbol{\alpha_j}) \frac{\cos(\omega_{ij} r_{ij})}{r_{ij}} \tag{7}$$

and the retardation interaction

$$V_{ij}^{\mathrm{ret}} = (\boldsymbol{\alpha_i} \cdot \boldsymbol{\nabla}_i)(\boldsymbol{\alpha_j} \cdot \boldsymbol{\nabla}_j) \frac{\cos(\omega_{ij} r_{ij}) - 1}{\omega_{ij}^2 r_{ij}}, \tag{8}$$

where the $\boldsymbol{\alpha}$ are Dirac matrices and r_{ij} and ω_{ij} are the interelectronic distance and the exchanged virtual photon energy divided by the speed of the light c between the ith and jth

electron, respectively. As $\omega_{ij} \to 0$, we refer to Eq. (5) as the BI [43,44].

The calculation of the alignment parameters $\mathcal{A}_k^s$ for the second-step radiative decay from state $|s\rangle$ to $|g\rangle$ requires a correction to the first-step radiative decay $\mathcal{A}_k^d$ as

$$\mathcal{A}_k^s = \mathcal{A}_k^d U_k(J_s, J_d, L). \tag{9}$$

Here the $U_k(J_s, J_d, L)$ is the deorientation factor [36], which can be expressed as

$$U_k(J_d, J_s, L) = (-1)^{J_d+J_s+k+L}(J_d, J_s)^{1/2}\begin{Bmatrix} J_d & J_d & k \\ J_s & J_s & L \end{Bmatrix}, \tag{10}$$

where $L = 1$ for $E1$ and magnetic dipole ($M1$) transitions and $L = 2$ for magnetic quadrupole ($M2$) transitions.

In addition, the density-matrix method can also calculate the alignment parameters of second-step radiative decay [37] and the $\mathcal{A}_{kq}^s$ can be written as

$$\mathcal{A}_{k_2q_2}^s = W_{1\mathrm{st}}^{-1} \sum_{k_1 k} g_{k_1k_2k}^{ds} \mathcal{A}_k^d \langle k_1 - q_2 k_2 q_2 | k 0\rangle Y_{k_1,-q_2}(\pi/2, 0), \tag{11}$$

where $W_{1\mathrm{st}}$ is the angular distribution coefficient of the first-step radiative decay and will be discussed in detail in the following section. Additionally, $Y_{k_1,-q_2}$ are the spherical harmonics and k_2 and k are the multipole orders of second-step and first-step radiative decays, respectively. For an atomic state with total angular momentum J, the multipole order k is restricted by $0 \leqslant k \leqslant 2J$, the projection q is restricted by $-k \leqslant q \leqslant k$, and the k_1 is restricted by $|k - k_2| \leqslant k_1 \leqslant k + k_2$. The alignment parameters of second-step radiative decay depend also on the so-called generalized structure function $g_{k_1k_2k}^{ds}$, which is defined as

$$g_{k_1k_2k}^{ds} = \mathcal{A}_k^d \frac{1}{4\sqrt{\pi}} (Jd, Js)^{1/2}[1 + (-1)^{k_1}](k_2, L, L)^{1/2} \times (-1)^{L+1}\langle L1L - 1|k_1 0\rangle \begin{Bmatrix} J_d & J_d & k \\ J_s & J_s & k_2 \\ L & L & k_1 \end{Bmatrix}, \tag{12}$$

…

where $\{\cdots\}$ is the Wigner 9-j symbol.

…

B. Angular distribution and polarization

The angular distribution and polarization directly depend on the alignment parameters. The differential cross section of a polarized target [45] can be expressed as

$$\sigma(\theta) = \frac{\sigma}{4\pi}\left(\sum_{k\geqslant 0} B_k P_k(\cos\theta) - \sum_{k\geqslant 2} \beta f_k B_k P_k^2(\cos\theta)\cos(2\phi)\right), \tag{13}$$

where P_k is the Legendre polynomial, P_k^2 is the associated Legendre polynomial, θ is the angle between the incident electron and the emitted photon, and ϕ is the azimuth angle of the polarization direction of the photon relative to the electron direction. The function β determines the sign: $\beta = 1$ for electric multipole transitions and $\beta = -1$ for magnetic multipole transitions. In addition, f_k is the coefficient for a particular transition

$$f_k(L) = -\left(\frac{(k-2)!}{(k+2)!}\right)^{1/2} \frac{\begin{pmatrix} L & L & k \\ 1 & 1 & -2 \end{pmatrix}}{\begin{pmatrix} L & L & k \\ 1 & -1 & 0 \end{pmatrix}} \tag{14}$$

and B_k is the angular anisotropy parameter

$$B_k = \alpha_k \mathcal{A}_k, \tag{15}$$

where $\begin{pmatrix} \cdots \\ \cdots \end{pmatrix}$ denotes the Wigner 3-j symbol and α_k is intrinsic anisotropy parameter [41], which can be expressed as

$$\alpha_k(J_d, J_s, L) = (-1)^{J_d+J_s-1}(k, J_d)^{1/2}(2L+1) \times \begin{pmatrix} L & L & k \\ 1 & -1 & 0 \end{pmatrix}\begin{Bmatrix} L & L & k \\ J_d & J_d & J_s \end{Bmatrix}. \tag{16}$$

Hence, the angular distribution coefficient can be expressed as

$$W(\theta) = \sum_{k\geqslant 0} B_k P_k(\cos\theta). \tag{17}$$

The linear polarization for the first-step radiative decay [45] can be expressed as

$$P(\theta) = \frac{\sigma_\parallel(\theta) - \sigma_\perp(\theta)}{\sigma_\parallel(\theta) + \sigma_\perp(\theta)} = \frac{\sum_{k\geqslant 2} \beta f_k B_k P_k^2(\cos\theta)}{\sum_{k\geqslant 0} B_k P_k(\cos\theta)}, \tag{18}$$

where $\sigma_\parallel$ and $\sigma_\perp$ are the cross sections for photons polarized in the direction parallel ($\phi = 0^\circ$) and perpendicular ($\phi = 90^\circ$) to the electron direction, respectively. In this work we focus on the dielectronic satellite lines of hydrogenlike ions in the direction perpendicular to the electron-beam axis (i.e., 90°); dipole and quadrupole transitions are the dominant transitions, so we can simplify the calculation of the angular distribution coefficient (17) as

$$W = 1 - \tfrac{1}{2}\alpha_2 \mathcal{A}_2 + \tfrac{3}{8}\alpha_4 \mathcal{A}_4. \tag{19}$$

The linear polarization (18) can be simplified as

$$P = \mp \frac{3\alpha_2 \mathcal{A}_2}{2 - \alpha_2 \mathcal{A}_2}. \tag{20}$$

Moreover, for quadrupole radiative transitions, the linear polarization can be written as

$$P = \pm \frac{12\alpha_2 \mathcal{A}_2 + 5\alpha_4 \mathcal{A}_4}{8 - (4\alpha_2 \mathcal{A}_2 - 3\alpha_4 \mathcal{A}_4)}. \tag{21}$$

For the first-step and second-step radiative decays, the corresponding $\alpha_2^{ds}\mathcal{A}_2^d$ and $\alpha_2^{sg}\mathcal{A}_2^s$ can be used in the calculation.

Similarly, if the density-matrix method is used to calculate the angular distribution coefficient and linear polarization,

they directly depend on the alignment parameters $\mathcal{A}^s_{kq}$ in Eq. (11) and the angular distribution coefficient of first-step radiative decay W_{1st}. The angular distribution coefficient can be written as [41]

$$W_{2nd} = W_{1st}\left(1 + \alpha_2^{sg}\sqrt{\frac{4\pi}{5}}\sum_{q=-2}^{2}\mathcal{A}^s_{2q}Y_{2q}(\pi/2,0) + \alpha_4^{sg}\sqrt{\frac{4\pi}{9}}\sum_{q=-4}^{4}\mathcal{A}^s_{4q}Y_{4q}(\pi/2,0)\right). \tag{22}$$

For the dipole radiative transitions, the linear polarization can be written as [41]

$$P = \mp\frac{\sqrt{\frac{3}{2}}\alpha_2^{sg}\sum_q \mathcal{A}^s_{2q}D_2}{1 + \alpha_2^{sg}\sqrt{\frac{4\pi}{5}}\sum_q \mathcal{A}^s_{2q}Y_{2q}(\pi/2,0)}, \tag{23}$$

where D_k denotes the Wigner D function

$$D_k = \left[D^{k*}_{q2}(0,\pi/2,0) + D^{k*}_{q-2}(0,\pi/2,0)\right]. \tag{24}$$

For the quadruple radiative transitions, the linear polarization can be written as [41]

$$P = \pm W_{2nd}^{-1}\left(\sqrt{\frac{3}{2}}\alpha_2^{sg}\sum_{q=-2}^{2}\mathcal{A}^s_{2q}D_2 - \sqrt{\frac{5}{8}}\alpha_4^{sg}\sum_{q=-4}^{4}\mathcal{A}^s_{4q}D_4\right). \tag{25}$$

The difference between the deorientation factor formalism and the density-matrix theory intrinsically stems from the different treatments for the second-step radiative decay $\mathcal{A}^s_k$. The $\mathcal{A}^s_k$ calculated by the deorientation factor directly depends on the first-step radiative decay $\mathcal{A}^d_k$ only and these two parameters demonstrate a simple linear relationship. In contrast, the calculation of $\mathcal{A}^s_{kq}$ using the density-matrix method depends on both $\mathcal{A}^d_k$ and the angular distribution coefficient of the first-step radiative decay. If the $q \neq 0$ components and the angular distribution coefficient of the first-step radiative decay are neglected in the calculation of angular distribution and polarization using the density-matrix method, the results of these two parameters should be consistent with the results calculated by the deorientation factor formalism. Hence, for the axial symmetry decay system, the deorientation factor formalism provides a simple and efficient method for calculating the angular distribution and polarization of the second-step radiative decay. However, for the complex decay system, the calculation results by the density-matrix method are more comprehensive than those by the deorientation factor formalism.

C. Resonance strengths and synthetic spectra of x-ray line emissions

The resonance strength of DR from an initial state $|i\rangle$, involving a doubly excited state $|d\rangle$, to a singly excited state $|s\rangle$ [46] can be expressed as

$$S_{ids} = \int_0^\infty \sigma_{ids}(E)dE = \frac{g_d}{2g_i}\frac{\pi^2\hbar^3 A^a_{di}}{m_e E_{res}}\frac{A^r_{ds}}{\sum A^r + \sum A^a}, \tag{26}$$

where $\hbar$ is the reduced Planck constant; m_e is the electron mass; E_{res} and A^a_{di} are the resonance energy and autoionization rate of states $|i\rangle$ and $|d\rangle$, respectively; A^r_{ds} is the Einstein coefficient for spontaneous emission from state $|d\rangle$ to state $|s\rangle$; g_d and g_i are statistical weights of states $|d\rangle$ and $|i\rangle$, respectively, which are the total angular momenta; and the summations in the denominator are the autoionization rates and Einstein coefficients of all possible channels for state $|d\rangle$. Note that the resonance strength of second-step radiative decay from state $|s\rangle$ to state $|g\rangle$ is the same as the first-step radiative decay from state $|d\rangle$ to state $|s\rangle$, except for some two-channel decays, which require consideration of the branching ratio. For instance, the singly excited state $(1s2p_{3/2})_2$ has two different channels to the ground state $(1s^2)_0$. One is the direct decay and the other is the state decaying first to $(1s2s)_1$ before decaying to the ground state.

To calculate the relative intensity of dielectronic satellite lines for comparison with the experimental spectrum, the angular distribution coefficient W must be considered. For measurements at EBITs, the relative intensity can be expressed as

$$I \propto S_{ids}W(90^\circ). \tag{27}$$

Due to the natural width of the energy level, the synthetic spectra have a Lorentz profile, which can be expressed as

$$L(E) = \frac{2}{\pi\Gamma}\frac{1}{1 + 4[(E - E_0)/\Gamma]^2}. \tag{28}$$

Here E_0 is the photon energy or resonant energy corresponding to the broadening in different energy directions and Γ is the natural width

$$\Gamma = \hbar\left(\sum A^r + \sum A^a\right), \tag{29}$$

where A^r and A^a are the Einstein coefficient and autoionization rate, respectively. In addition, the energy broadening of the photon and electron can be described by the Gaussian profile as

$$G(E) = \frac{1}{\omega\sqrt{\pi/2}}\exp\left(\frac{-2(E - E_0)^2}{\omega^2}\right), \tag{30}$$

where ω is the energy resolution. Actually, one can use a Voigt profile to describe the contribution of these two profiles, which can be expressed as

$$V(E) = \frac{2\ln 2}{\pi\sqrt{\pi}}\frac{\Gamma}{\omega^2} \times \int_{-\infty}^{\infty}\frac{e^{-t^2}}{[2\sqrt{\ln 2}(E - E_0)/\omega - t]^2 + (\sqrt{\ln 2}\Gamma/\omega)^2}dt, \tag{31}$$

and then the synthetic spectra can be expressed as

$$F(E) = \sum IV(E). \tag{32}$$

In the following calculations we use the spectra measured on the. free-electron laser in Hamburg (FLASH) EBIT [14] and Tokyo EBIT [30] as references. We set the photon energy broadening to 3.2 keV for Ti^{21+}, Kr^{35+}, and Mo^{41+} ions and

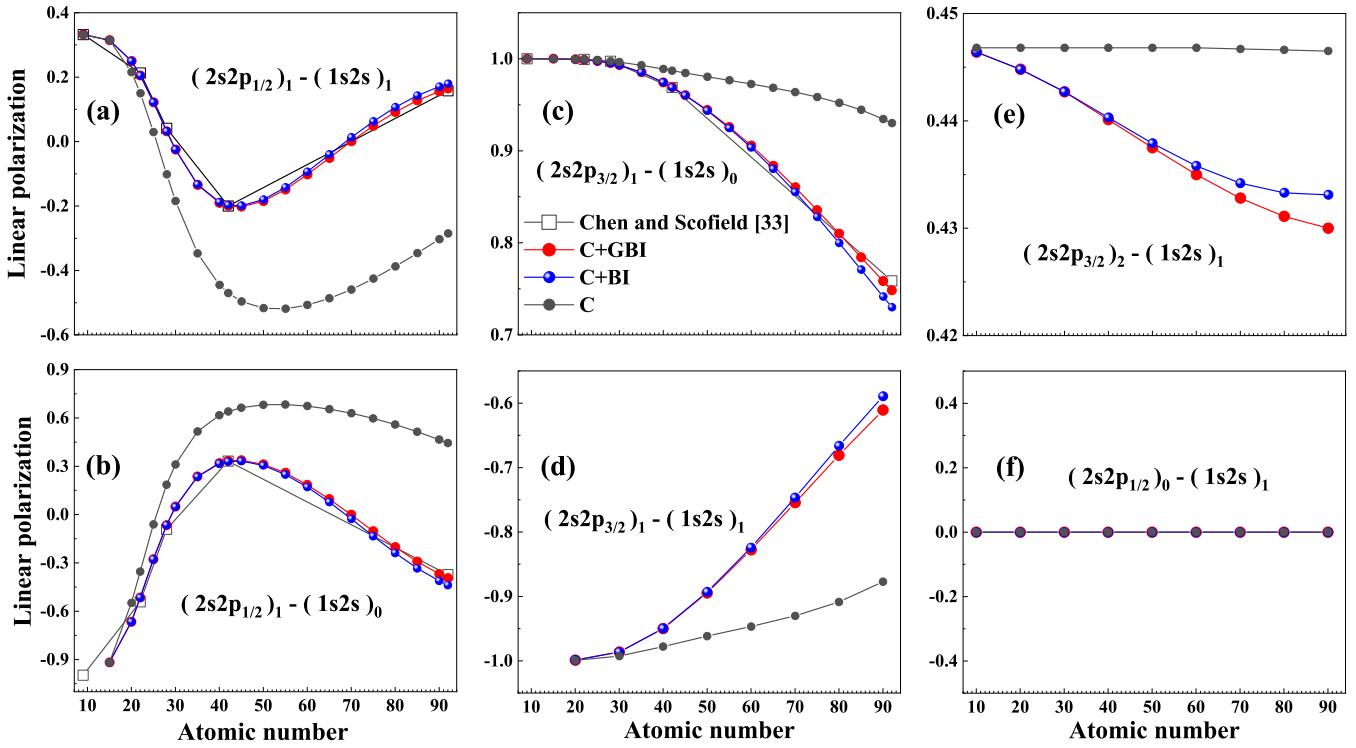

FIG. 1. Atomic number dependence of the degree of linear polarization for the hydrogenlike satellite lines from configuration $2s2p$ to $1s2s$. The red circles are the calculations performed with GBI included, the blue circles are with BI included, and the black circles are the Coulomb interaction (C) only. The open squares in (a)–(c) are the calculation results from the work of Chen and Scofield [33].

4.7 keV for U^{91+} ions. The electron energy broadening is set to 60 eV.

III. RESULTS AND DISCUSSION

A. Calculation of linear polarization

In this section we focus on the linear polarization of first-step radiative decay. Figure 1 shows the calculated linear polarization of dielectronic satellite lines of hydrogenlike ions from configuration $2s2p$ to $1s2s$, i.e., $(2s2p_{1/2})_1 \rightarrow (1s2s)_{0,1}$, $(2s2p_{3/2})_1 \rightarrow (1s2s)_{0,1}$, and $(2s2p_{3/2})_2 \rightarrow (1s2s)_1$. As can be seen from Figs. 1(a) and 1(b), the present linear polarizations

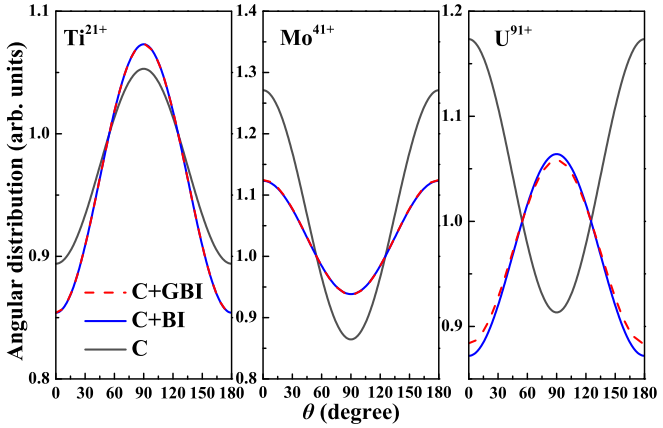

FIG. 2. Angular distribution of $(2s2p_{1/2})_1 \rightarrow (1s2s)_1$ of Ti^{21+}, Mo^{41+}, and U^{91+} ions.

with GBI are in excellent agreement with those obtained by Chen and Scofield [33]. The difference in linear polarizations between the calculations with GBI and BI is small and only slightly different for high-Z ions. However, the difference between BI and the Coulomb interaction only is significant, and this difference gradually increases with increasing atomic number Z. For the transitions sharing the same doubly excited state but differing in the total angular momentum of the singly excited state, i.e., $(2s2p_{1/2})_1 \rightarrow (1s2s)_1$ [Fig. 1(a)], $(2s2p_{1/2})_1 \rightarrow (1s2s)_0$ [Fig. 1(b)], and $(2s2p_{3/2})_1 \rightarrow (1s2s)_0$ [Fig. 1(c)], $(2s2p_{3/2})_1 \rightarrow (1s2s)_1$ [Fig. 1(d)], the effects of BI and GBI show a similar feature. However, these transitions demonstrate completely opposite polarization behaviors, which poses a challenge for experimental measurements.

For the transitions $(2s2p_{1/2})_1 \rightarrow (1s2s)_1$ and $(2s2p_{1/2})_1 \rightarrow (1s2s)_0$, the linear polarization does not exhibit a monotonic variation with atomic number Z, which is different from other transitions. Notably, the monotonicity of these two transitions experiences a significant change at $Z = 42$ when BI and GBI are considered. Furthermore, the polarization behaviors of these two transitions are qualitatively altered at $Z = 70$ due to the contributions of BI and GBI. Similarly, the angular distribution behavior also illustrates the effects of BI and GBI. For instance, in the transitions $(2s2p_{1/2})_1 \rightarrow (1s2s)_1$ of high-Z ($Z \geqslant 70$) ions, the angular distributions of emitted photons with the Coulomb interaction only are predominantly radiated at $\theta = 0^\circ$ and 180°. However, the angular distribution behavior becomes quite different when BI and GBI are taken into consideration. Figure 2 shows the angular distributions of $(2s2p_{1/2})_1 \rightarrow (1s2s)_1$ of Ti^{21+}, Mo^{41+}, and U^{91+} ions and

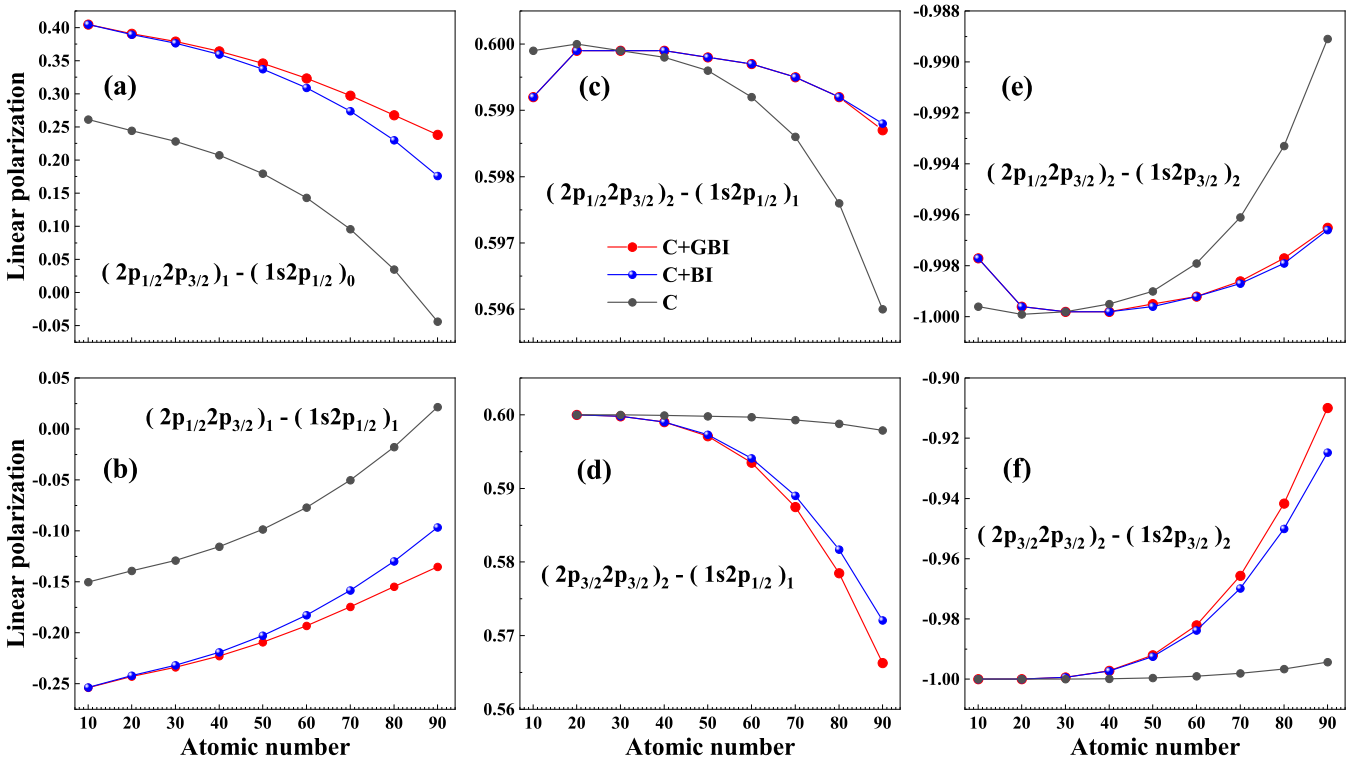

FIG. 3. Similar to Fig. 1 but from configuration $2p^2$ to $1s2p$.

the qualitative change can also be found in U^{91+} ions. Such a qualitative change was obtained also for the angular distribution of x-ray lines following electron-impact excitation of hydrogenlike ions [47] and dielectron recombination of lithiumlike ions [8].

The contribution of BI for the transition $(2s2p_{3/2})_2 \rightarrow (1s2s)_1$ [Fig. 1(e)] is less than 5% even for high-Z ions, while BI plays a more substantial role for other transitions. Specially, the emission photons of the transition with zero total angular momentum of the doubly excited state, for example, $(2s2p_{1/2})_0 \rightarrow (1s2s)_1$ [Fig. 1(f)], are unpolarized due to intrinsic anisotropy parameter being zero in Eq. (20).

To further account for the detailed calculation of the linear polarization of hydrogenlike dielectron satellite lines, the transitionsfrom configuration $2p^2$ to $1s2p$ are also calculated, as shown in Fig. 3. The effect of BI for the transitions

TABLE I. Present calculations of angular anisotropy parameters of dielectronic satellite lines of hydrogenlike Ti^{21+}, Mo^{41+}, and U^{91+} ions, as well as the theoretical results from the work of Chen and Scofield [33].

Transition		Ti^{21+}				Mo^{41+}				U^{91+}			
$\|d\rangle$	$\|s\rangle$	C	C+BI	C+GBI	Ref.	C	C+BI	C+GBI	Ref.	C	C+BI	C+GBI	Ref.
$(2s2p_{1/2})_1$	$(1s2s)_1$	−0.106	−0.146	−0.146	−0.153	0.271	0.123	0.125	0.125	0.173	−0.128	−0.116	−0.111
	$(1s2s)_0$	0.211	0.293	0.293	0.306	−0.542	−0.246	−0.250	−0.249	−0.346	0.255	0.232	0.221
$(2s2p_{3/2})_2$	$(1s2s)_1$	−0.350	−0.348	−0.348	−0.348	−0.350	−0.344	−0.344	−0.343	−0.350	−0.338	−0.334	−0.334
$(2p_{1/2}2p_{3/2})_1$	$(1s2p_{1/2})_0$	−0.176	−0.296	−0.298	−0.303	−0.144	−0.274	−0.274	−0.271	−0.020	−0.116	−0.168	−0.159
	$(1s2p_{1/2})_1$	0.088	0.148	0.149	0.152	0.072	0.134	0.137	0.136	0.041	0.058	0.084	0.080
	$(1s2p_{1/2})_2$	−0.018	−0.030	−0.030	−0.030	−0.014	−0.026	−0.028	−0.027	0.004	−0.012	−0.016	−0.016
	$(1s2p_{3/2})_1$	0.088	0.148	0.149	0.152	0.072	0.134	0.137	0.136	−0.020	0.058	0.084	0.080
$(2p_{1/2}2p_{3/2})_2$	$(1s2p_{1/2})_1$	−0.500	−0.500	−0.500	−0.500	−0.500	−0.500	−0.500	−0.500	−0.496	−0.498	−0.498	−0.499
	$(1s2p_{3/2})_2$	0.500	0.500	0.500	0.500	0.500	0.500	0.500	0.500	0.495	0.499	0.499	0.499
	$(1s2p_{3/2})_1$	−0.500	−0.500	−0.500	−0.500	−0.500	−0.500	−0.500	−0.500	−0.496	−0.498	−0.498	−0.499
$(2p_{3/2}2p_{3/2})_2$	$(1s2p_{1/2})_1$	−0.500	−0.500	−0.500	−0.500	−0.500	−0.498	−0.498	−0.499	−0.498	−0.470	−0.462	−0.462
	$(1s2p_{1/2})_2$	0.500	0.500	0.500	0.500	0.500	0.499	0.499	0.499	0.498	0.469	0.463	0.462
	$(1s2p_{3/2})_1$	−0.500	−0.500	−0.500	−0.500	−0.500	−0.498	−0.498	−0.499	−0.498	−0.470	−0.462	−0.462
$(2s2p_{3/2})_1$	$(1s2s)_1$	0.499	0.499	0.499	0.499	0.490	0.477	0.477	0.477	0.449	0.322	0.332	0.338
	$(1s2s)_0$	−0.998	−0.998	−0.998	−0.999	−0.980	−0.954	−0.954	−0.954	−0.898	−0.644	−0.664	−0.677

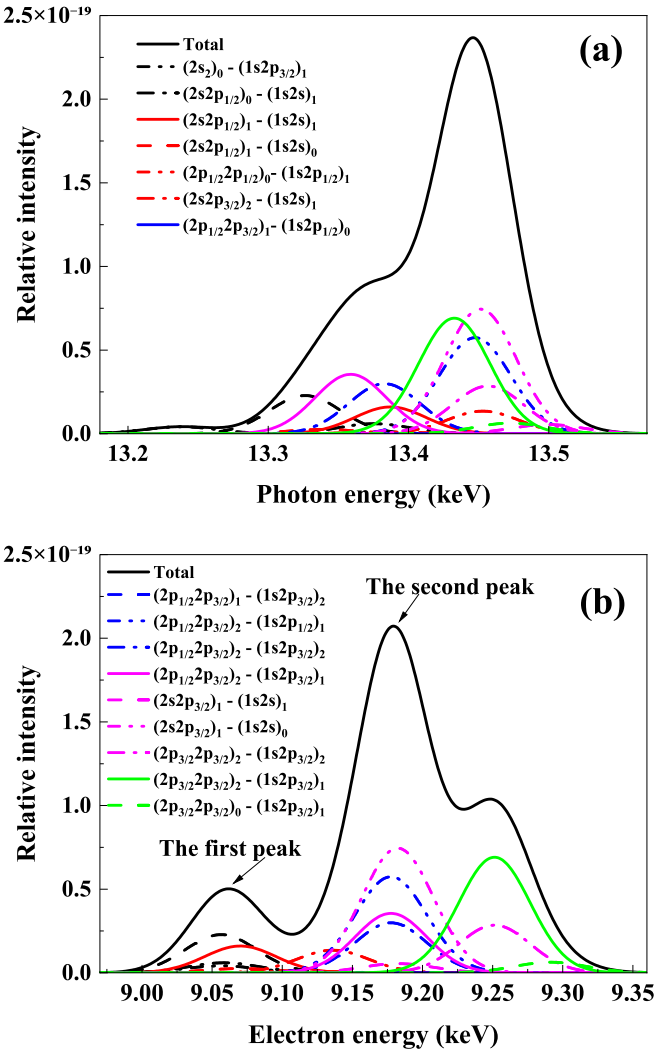

FIG. 4. Relative intensity of dielectronic satellite lines of hydrogenlike Kr^{35+} ions corresponding to the first-step radiative decay photons. The colored lines show the spectra associated with individual transitions, while the black solid line indicates the overall spectra.

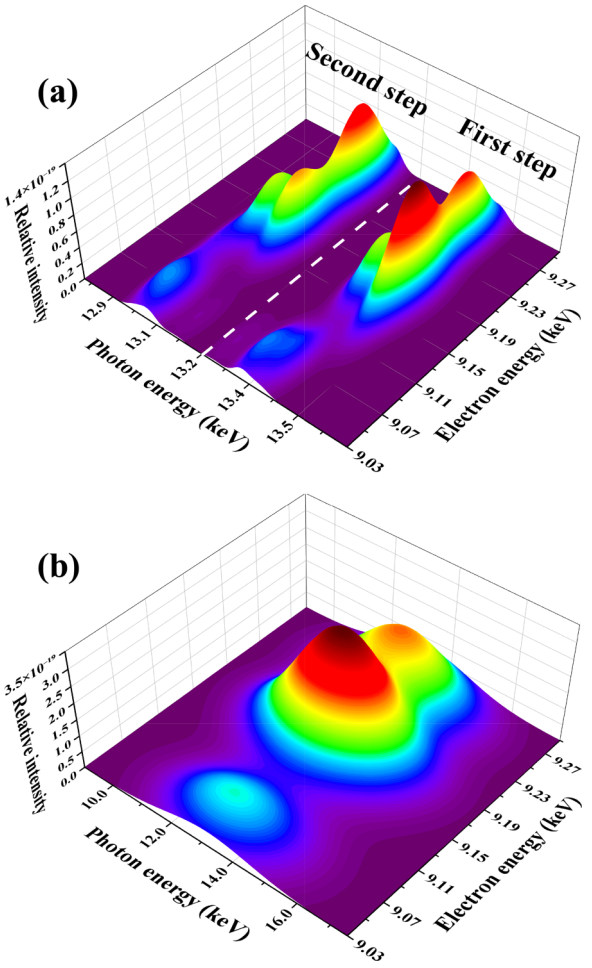

FIG. 5. Relative intensity of dielectronic satellite lines of hydrogenlike Kr^{35+} ions including the first-step radiative decay and second-step radiative decay photons. The broadenings are (a) 60 eV and (b) 3.2 keV in the photon energy direction.

of the doubly excited state $(2p_{1/2}2p_{3/2})_1$ is independent of the atomic number Z, such as $(2p_{1/2}2p_{3/2})_1 \rightarrow (1s2p_{1/2})_0$ [Fig. 3(a)] and $(2p_{1/2}2p_{3/2})_1 \rightarrow (1s2p_{1/2})_1$ [Fig. 3(b)]. The BI effect of these transitions does not significantly change with increasing atomic number Z, which is dissimilar from other dielectronic satellite lines of hydrogenlike ions. Note that the transition $(2p_{1/2}2p_{3/2})_1 \rightarrow (1s2p_{1/2})_2$ is almost unpolarized, and thus it is not presented here. The variations of linear polarization for the transitions of doubly excited states $(2p_{1/2}2p_{3/2})_2$ and $(2p_{3/2}2p_{3/2})_2$ remain negligible (less than 0.1) with increasing Z, as shown in Figs. 3(c)–3(f). In addition, the transitions that have the same doubly excited states, e.g., $(2p_{1/2}2p_{3/2})_2$ and $(2p_{3/2}2p_{3/2})_2$, but different singly excited states $(1s2p_{1/2})_1$ and $(1s2p_{3/2})_1$ have the same polarization behaviors; thus only the transitions with the singly excited state $(1s2p_{1/2})_1$ are shown here. The detailed polarization values of $Z = 22$, 42, and 92 are listed in Table I. The linear polarization with GBI in our investigation exhibit excellent agreement with those obtained by Chen and Scofield [33].

B. Synthetic spectra

In this section we perform the calculations for the relative intensity of dielectronic satellite lines in both the first-step and second-step radiative decays, taking into account the contribution of BI. Here the transitions with higher resonance strengths are focused on, and the contributions of other transitions with resonance strengths smaller than 1×10^{-22} are nearly negligible.

Figure 4 shows the calculated relative intensity of dielectronic satellite lines during the first-step radiative decay of hydrogenlike Kr^{35+} ions. For a clear display, the broadening here is 60 eV for both the photon and electron energy directions. As evident from the figure, 17 peaks are found in the synthetic spectra. Even with a 60-eV broadening in the photon energy direction, it is challenging to distinguish these peaks, as shown in Fig. 4(a). The transitions with higher intensities and significant polarization behaviors are considered. Four transitions are picked out, i.e.,

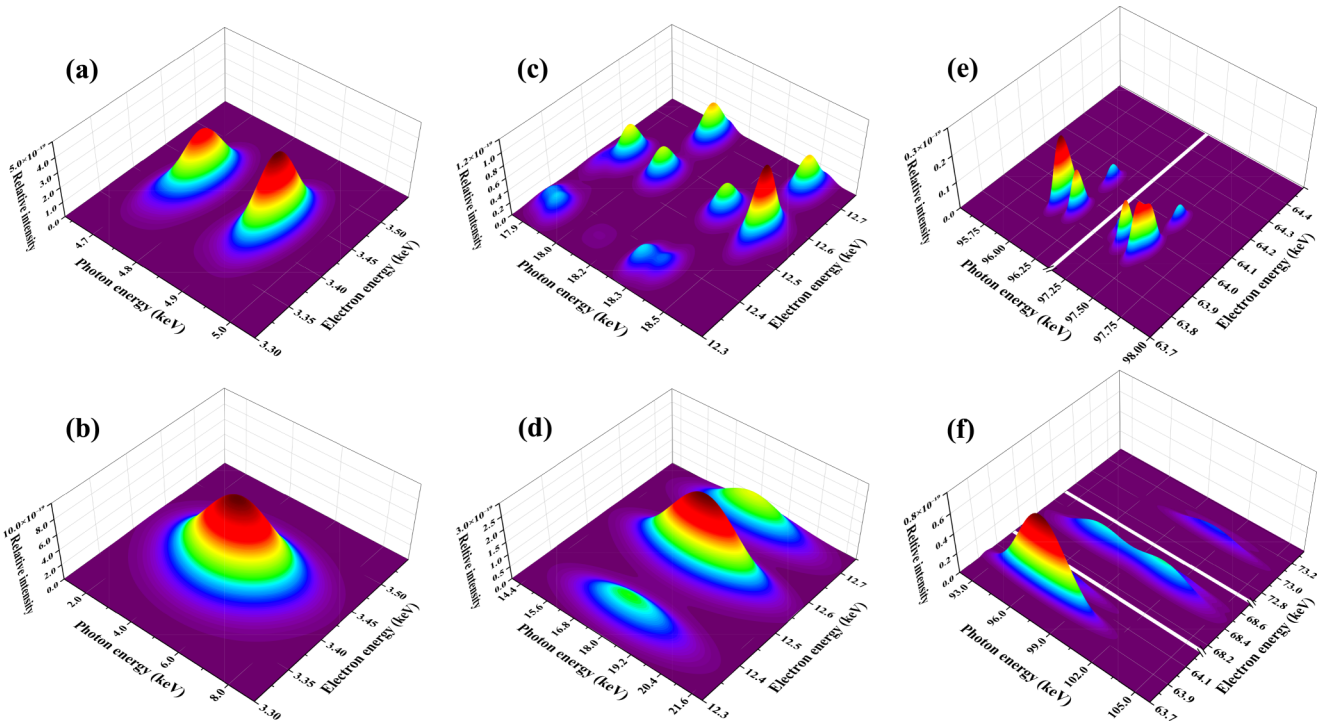

FIG. 6. Similar to Fig. 5 but for (a) and (b) Ti^{21+}, (c) and (d) Mo^{41+}, and (e) and (f) U^{91+} ions.

$(2s2p_{1/2})_1 \rightarrow (1s2s)_1$, $(2s2p_{1/2})_1 \rightarrow (1s2s)_0$, $(2s2p_{3/2})_1 \rightarrow (1s2s)_1$, and $(2s2p_{3/2})_1 \rightarrow (1s2s)_0$. As shown in Fig. 4(b), two of these transitions are in the first broad peak and the other two are in the second broad peak in the electron energy direction. In the following, the first peak and the second peak refer to the first and second broad peaks, respectively, in the electron energy direction, unless stated otherwise.

The relative intensity of dielectronic satellite lines of hydrogenlike Kr^{35+} ions, including first-step and second-step radiative decays, is also calculated as shown in Fig. 5. For a clear display, a broadening of 60 eV is used in Fig. 5(a) for both photon and electron energy directions. Two areas can be seen in the photon energy direction, corresponding to the two-step radiative decays with an energy difference of around

TABLE II. Calculated resonance energy $E_{\rm res}$, photon energy $h\nu$, angular distribution coefficient W at 90°, relative intensity I, and branching ratio B.

$\|d\rangle$	$\|s\rangle$	$E_{\rm res}$	$h\nu_1$	$W_{\rm 1st}$	$I_{\rm 1st}$	$\|g\rangle$	$h\nu_2$	B	$W_{\rm 2nd}(U)$	$W_{\rm 2nd}$	$I_{\rm 2nd}(U)$	$I_{\rm 2nd}$
$(2s^2)_0$	$(1s2p_{1/2})_1$	9056.3	13326.3	1	2.275	$(1s^2)_0$	13025.1	1	1	1	2.275	2.275
	$(1s2p_{3/2})_1$	9056.3	13237.6	1	0.418	$(1s^2)_0$	13113.9	1	1	1	0.418	0.418
$(2s2p_{1/2})_0$	$(1s2s)_1$	9058.5	13375.4	1	0.597	$(1s^2)_0$	12978.1	1	1	1	0.597	0.597
$(2s2p_{1/2})_1$	$(1s2s)_1$	9070.1	13387.1	0.953	1.597	$(1s^2)_0$	12978.1	1	0.953	0.945	1.597	1.584
	$(1s2s)_0$	9070.1	13339.1	1.094	0.254							
$(2p_{1/2}2p_{1/2})_0$	$(1s2p_{1/2})_1$	9113.5	13383.5	1	0.109	$(1s^2)_0$	13025.1	1	1	1	0.109	0.109
$(2s2p_{3/2})_2$	$(1s2s)_1$	9136.0	13453.0	1.172	1.355	$(1s^2)_0$	12978.1	1	1.172	1.187	1.355	1.373
$(2p_{1/2}2p_{3/2})_1$	$(1s2p_{1/2})_0$	9166.3	13439.0	1.139	0.018							
	$(1s2p_{3/2})_2$	9166.3	13371.6	1.014	0.019	$(1s^2)_0$	13089.8	0.902	0.930	0.996	0.016	0.017
		9166.3	13371.6	1.014	0.019	$(1s2s)_1 \rightarrow (1s^2)_0$	111.7	0.098	1.049	1.018	0.002	0.002
$(2p_{1/2}2p_{3/2})_2$	$(1s2p_{1/2})_1$	9177.5	13447.5	1.250	5.741	$(1s^2)_0$	13025.1	1	1.250	1.296	5.741	5.950
	$(1s2p_{3/2})_2$	9177.5	13382.8	0.750	2.988	$(1s^2)_0$	13089.8	0.902	1.250	0.820	4.491	2.945
		9177.5	13382.8	0.750	2.988	$(1s2s)_1 \rightarrow (1s^2)_0$	111.7	0.098	1.125	0.749	0.439	0.292
	$(1s2p_{3/2})_1$	9177.5	13358.8	1.250	3.548	$(1s^2)_0$	13113.9	1	1.250	1.296	3.548	3.678
$(2s2p_{3/2})_1$	$(1s2s)_1$	9182.3	13499.3	0.756	0.548	$(1s^2)_0$	12978.1	1	0.756	0.717	0.548	0.519
	$(1s2s)_0$	9182.3	13451.3	1.488	7.448							
$(2p_{3/2}2p_{3/2})_2$	$(1s2p_{3/2})_2$	9251.3	13456.7	0.750	2.851	$(1s^2)_0$	13089.8	0.902	1.250	0.820	4.278	2.809
		9251.3	13456.7	0.750	2.851	$(1s2s)_1 \rightarrow (1s^2)_0$	111.7	0.098	1.125	0.749	0.419	0.279
	$(1s2p_{3/2})_1$	9251.3	13432.7	1.250	6.913	$(1s^2)_0$	13113.9	1	1.250	1.295	6.913	7.164
$(2p_{3/2}2p_{3/2})_0$	$(1s2p_{3/2})_1$	9291.3	13472.6	1	0.634	$(1s^2)_0$	13113.9	1	1	1	0.634	0.634

several hundred eVs. However, the energy resolution of the Compton camera installed on the FLASH EBIT and Tokyo EBIT are 3.2 keV at 13 keV [14] and 4.7 keV at 81 keV [30], respectively, which is not sufficient to separate these two-step decays. The measured spectrum would correspond to Fig. 5(b), which has a broadening of 3.2 keV in the photon energy direction.

Similarly, Fig. 6 shows the relative intensity of dielectronic satellite lines of hydrogenlike Ti^{21+}, Mo^{41+}, and U^{91+} ions. In the case of Ti^{21+} ions, all the transitions merge into a single peak; it is difficult to distinguish these transitions in the photon and electron energy directions. However, as the atomic number Z increases, such as for Kr^{35+} and Mo^{41+} ions, three peaks can be distinguished in the electron energy direction. This distinction becomes even more pronounced for U^{91+} ions, where even two-step radiative decays can be distinguished in the photon energy direction. Notably, for a clear display, the first peak of the transitions of U^{91+} ions is shown in Fig. 6(e). As shown in Eq. (27), the relative intensity also depends on the angular distribution coefficient W. The detailed calculations of the relative intensities of these transitions as listed in Table II are beneficial for calculating the effective polarization.

Three transitions in the second-step radiative decay are further discussed here. The transitions $(1s2s)_0 \to (1s^2)_0$ and $(1s2p_{1/2})_0 \to (1s^2)_0$ are strictly forbidden by the selection rule, which follows from the fact that photons have spin 1 and thus transport a quantum of angular momentum. In particular, the two-photon decay transition $(1s2s)_0 \to (1s^2)_0$ is discussed in Sec. II. In addition, the singly excited state $(1s2p_{3/2})_2$ has two decay channels to the ground state $(1s^2)_0$. One involves a two-step transition $(1s2p_{3/2})_2 \to (1s2s)_1 \to (1s^2)_0$, while the other is a direct transition $(1s2p_{3/2})_2 \to (1s^2)_0$. Therefore, the branching ratio of these two channels should be considered. In the first case, only the transition $(1s2s)_1 \to (1s^2)_0$ can contribute to the synthetic spectra, because the photon energy of the other transition $(1s2p_{3/2})_2 \to (1s2s)_1$ is too low.

For comparison with the experimental measurements, the effective polarization should be considered as

$$P_{\text{effect}} = \frac{\sum_i P_i I_i}{\sum_i I_i}, \tag{33}$$

where P_i and I_i are the linear polarization and relative intensity of the transition i, respectively. However, as shown in Figs. 4 and 5, there is a significant overlap of multiple transitions within the second peak, which makes it difficult to discuss the effective polarization. Therefore, the first peak which includes six transitions is first investigated in this work. Among these, two transitions exhibit significant polarization behaviors, i.e., $(2s2p_{1/2})_1 \to (1s2s)_1$ and $(2s2p_{1/2})_1 \to (1s2s)_0$, as shown in Figs. 1(a) and 1(b), respectively. Here we discuss three points in the calculation of effective polarization for these dielectronic satellite lines of hydrogen ions. First, the relative intensity of $(2s^2)_0 \to (1s2p_{3/2})_1$ is too small for the high-Z ($Z > 60$) ions to be negligible. Second, for high-Z ions, the energy resolution in the electron energy direction is sufficient to distinguish the transition $(2p_{1/2}^2)_0 \to (1s2p_{1/2})_1$, making it unnecessary to consider this transition in the calculation

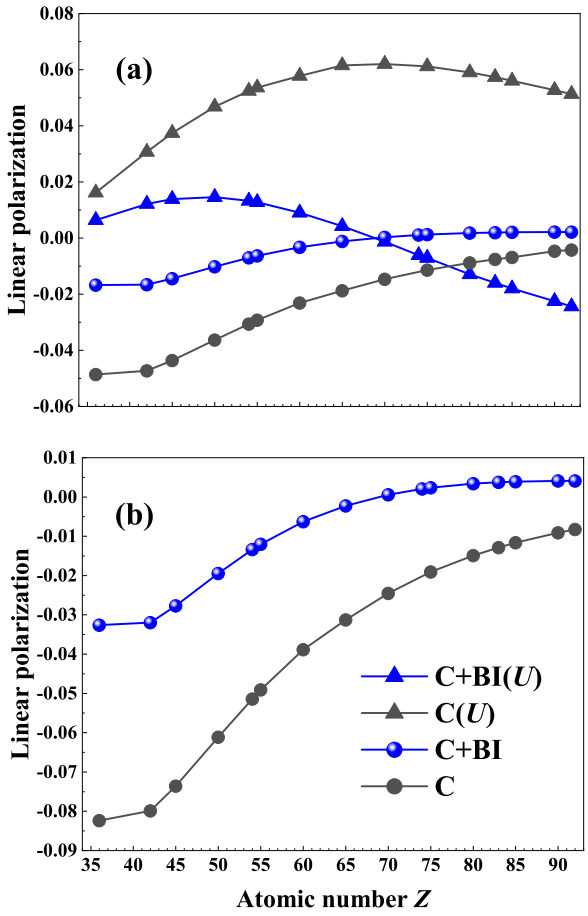

FIG. 7. Effective polarization of the first broad peak in the electron energy direction. The effective polarization is shown for both (a) two-step radiative decays and (b) only the first-step radiative decay.

of effective polarization. Note that for an atomic number Z higher than 90, e.g., for U^{91+}, the distinguishable transition transforms into $(2s^2)_0 \to (1s2p_{1/2})_1$. Third, the mixing of different multipoles in the expansion of electron-photon interaction operators for the radiative deexcitation process is considered. For the x rays from the transition $(2s2p_{1/2})_1 \to (1s2s)_1$ considered in the effective polarization, the $E1 + M2$ mixing is negligible for ions with Z values ranging from 9 to 92 [48].

Figure 7 shows the effective polarization for the first peak. Despite the significant polarization behavior and BI effect observed in the transitions $(2s2p_{1/2})_1 \to (1s2s)_1$ and $(2s2p_{1/2})_1 \to (1s2s)_0$, the overall effective polarization remains relatively insignificant. This is primarily due to the fact that these two transitions demonstrate completely opposite polarization behaviors as shown in Figs. 1(a) and 1(b), which poses a challenge for accurate experimental measurements. To address this issue, coincidence measurements could be employed to distinguish the two-step radiative decays, thereby enhancing the significance of the observed polarization behavior [49]. Additionally, the uncertainty of the EBIT Compton camera [30] can achieve 2%, which presents a promising opportunity for experimental validation and further

understanding of the BI effect and the difference between the formalism of the deorientation factor and the density-matrix theory of dielectronic satellite lines in hydrogenlike ions.

IV. SUMMARY

A systematic investigation of dielectronic satellite lines in hydrogenlike ions with Z values ranging from 9 to 92 was carried out and the effects of the Breit interaction and generalized Breit interaction on the linear polarization of satellite lines of those ions were discussed. The present results are in good agreement with those by Chen and Scofield [33]. Further, the polarization behavior was thoroughly discussed. In addition, the resonance strengths of the satellite lines were used to synthesize the dielectronic satellite line spectra with the experimental conditions of present-day electron-beam ion traps, such as the Tokyo EBIT.

Particular attention was paid to the two-step radiative decay process in dielectronic recombination of hydrogenlike Ti^{21+}, Kr^{35+}, Mo^{41+}, and U^{91+} ions. The alignment parameters of the second-step radiative decay were calculated using two methods, specifically the formalism of the deorientation factor and the density-matrix theory. Effective polarization calculations were performed by combining the polarization and synthetic spectra.

From the results obtained, it is evident that with the advancement of present-day EBITs, there is a promising opportunity to further understand the effect of the Breit interaction, as well as to distinguish the difference between the formalism of the deorientation factor and the density-matrix theory via the measurement of effective polarization of dielectronic satellite lines of hydrogenlike ions.

ACKNOWLEDGMENTS

This work was supported by the National Key R&D Program of China (Grant No. 2022YFA1602500), the Sichuan Science and Technology Program (Grant No. 2023ZYD0017), the National Natural Science Foundation of China (Grants No. 12074352, No. 12374234, and No. 12304275), and the Fundamental Research Funds for the Central Universities in China (Grant No. YJ202144).

[1] T. Watanabe, Spectroscopy of highly charged ions in solar and astrophysical plasmas, J. Phys.: Conf. Ser. **163**, 012002 (2009).

[2] F. Aharonian, H. Akamatsu, F. Akimoto, S. W. Allen, N. Anabuki, L. Angelini, K. Arnaud, M. Audard, H. Awaki, M. Axelsson, A. Bamba, M. Bautz, R. Blandford, L. Brenneman, G. V. Brown, E. Bulbul, E. Cackett, M. Chernyakova, M. Chiao, P. Coppi *et al.*, The quiescent intracluster medium in the core of the perseus cluster, Nature (London) **535**, 117 (2016).

[3] S. V. Vadawale, T. Chattopadhyay, N. P. S. Mithun, A. R. Rao, D. Bhattacharya, A. Vibhute, V. B. Bhalerao, G. C. Dewangan, R. Misra, B. Paul, A. Basu, B. C. Joshi, S. Sreekumar, E. Samuel, P. Priya, P. Vinod, and S. Seetha, Phase-resolved x-ray polarimetry of the Crab pulsar with the AstroSat CZT Imager, Nat. Astron. **2**, 50 (2018).

[4] Q. Abarr, H. Awaki, M. Baring, R. Bose, G. De Geronimo, P. Dowkontt, M. Errando, V. Guarino, K. Hattori, K. Hayashida, F. Imazato, M. Ishida, N. Iyer, F. Kislat, M. Kiss, T. Kitaguchi, H. Krawczynski, L. Lisalda, H. Matake, Y. Maeda *et al.*, XL-Calibur—a second-generation balloon-borne hard x-ray polarimetry mission, Astropart. Phys. **126**, 102529 (2021).

[5] R. Taverna, W. Zhang, M. Dovčiak, S. Bianchi, M. Bursa, V. Karas, and G. Matt, Towards a complete description of spectra and polarization of black hole accretion discs: Albedo profiles and returning radiation, Mon. Not. R. Astron. Soc. **493**, 4960 (2020).

[6] C. H. Skinner, Atomic physics in the quest for fusion energy and iter, Phys. Scr. **T134**, 014022 (2009).

[7] H. Feng, H. Li, X. Long, R. Bellazzini, E. Costa, Q. Wu, J. Huang, W. Jiang, M. Minuti, and W. Wang, Re-detection and a possible time variation of soft x-ray polarization from the Crab, Nat. Astron. **4**, 511 (2020).

[8] S. Fritzsche, A. Surzhykov, and T. Stöhlker, Dominance of the Breit interaction in the x-ray emission of highly charged ions following dielectronic recombination, Phys. Rev. Lett. **103**, 113001 (2009).

[9] Z. Hu, X. Han, Y. Li, D. Kato, X. Tong, and N. Nakamura, Experimental demonstration of the Breit interaction which dominates the angular distribution of x-ray emission in dielectronic recombination, Phys. Rev. Lett. **108**, 073002 (2012).

[10] Z. Hu, Y. Li, and N. Nakamura, Resonance strength for *KLL* dielectronic recombination of hydrogenlike krypton, Phys. Rev. A **87**, 052706 (2013).

[11] G. Xiong, J. Zhang, Z. Hu, N. Nakamura, Y. Li, X. Han, J. Yang, and B. Zhang, *KLL* dielectronic-recombination measurement for Li-like to O-like gold, Phys. Rev. A **88**, 042704 (2013).

[12] Z. Hu, Y. Li, X. Han, D. Kato, X. Tong, H. Watanabe, and N. Nakamura, Atomic-number dependence of the magnetic-sublevel population in the autoionization state formed in dielectronic recombination, Phys. Rev. A **90**, 062702 (2014).

[13] H. Jörg, Z. Hu, H. Bekker, M. A. Blessenohl, D. Hollain, S. Fritzsche, A. Surzhykov, J. R. Crespo López-Urrutia, and S. Tashenov, Linear polarization of x-ray transitions due to dielectronic recombination in highly charged ions, Phys. Rev. A **91**, 042705 (2015).

[14] C. Shah, H. Jörg, S. Bernitt, S. Dobrodey, R. Steinbrügge, C. Beilmann, P. Amaro, Z. Hu, S. Weber, S. Fritzsche, A. Surzhykov, J. R. Crespo López-Urrutia, and S. Tashenov, Polarization measurement of dielectronic recombination transitions in highly charged krypton ions, Phys. Rev. A **92**, 042702 (2015).

[15] R. Anholt, S. A. Andriamonje, E. Morenzoni, C. Stoller, J. D. Molitoris, W. E. Meyerhof, H. Bowman, J. S. Xu, Z. Z. Xu, J. O. Rasmussen, and D. H. H. Hoffmann, Observation of radiative capture in relativistic heavy-ion–atom collisions, Phys. Rev. Lett. **53**, 234 (1984).

[16] A. Ichihara, T. Shirai, and J. Eichler, Radiative electron capture in relativistic atomic collisions, Phys. Rev. A **49**, 1875 (1994).

[17] T. Stöhlker, C. Kozhuharov, P. H. Mokler, A. Warczak, F. Bosch, H. Geissel, R. Moshammer, C. Scheidenberger, J. Eichler, A. Ichihara, T. Shirai, Z. Stachura, and P. Rymuza, Radiative electron capture studied in relativis-

tic heavy-ion–atom collisions, Phys. Rev. A **51**, 2098 (1995).

[18] J. Eichler, A. Ichihara, and T. Shirai, Photon angular distributions from radiative electron capture in relativistic atomic collisions, Phys. Rev. A **51**, 3027 (1995).

[19] T. Stöhlker, T. Ludziejewski, F. Bosch, R. W. Dunford, C. Kozhuharov, P. H. Mokler, H. F. Beyer, O. Brinzanescu, B. Franzke, J. Eichler, A. Griegal, S. Hagmann, A. Ichihara, A. Krämer, J. Lekki, D. Liesen, F. Nolden, H. Reich, P. Rymuza, Z. Stachura *et al.*, Angular distribution studies for the time-reversed photoionization process in hydrogenlike uranium: The identification of spin-flip transitions, Phys. Rev. Lett. **82**, 3232 (1999).

[20] A. Surzhykov, S. Fritzsche, T. Stöhlker, and S. Tachenov, Polarization studies on the radiative recombination of highly charged bare ions, Phys. Rev. A **68**, 022710 (2003).

[21] J. R. Henderson, P. Beiersdorfer, C. L. Bennett, S. Chantrenne, D. A. Knapp, R. E. Marrs, M. B. Schneider, K. L. Wong, G. A. Doschek, J. F. Seely, C. M. Brown, R. E. LaVilla, J. Dubau, and M. A. Levine, Polarization of x-ray emission lines from heliumlike scandium as a probe of the hyperfine interaction, Phys. Rev. Lett. **65**, 705 (1990).

[22] A. Surzhykov, Y. Litvinov, T. Stöhlker, and S. Fritzsche, Hyperfine-induced effects on the linear polarization of $K\alpha_1$ emission from heliumlike ions, Phys. Rev. A **87**, 052507 (2013).

[23] Z. W. Wu, A. Surzhykov, and S. Fritzsche, Hyperfine-induced modifications to the angular distribution of the $K\alpha_1$ x-ray emission, Phys. Rev. A **89**, 022513 (2014).

[24] Z. W. Wu, Z. Q. Tian, J. Jiang, C. Z. Dong, and S. Fritzsche, Hyperfine-induced effects on angular emission of the magnetic-quadrupole line $1s2p_{3/2}\,{}^3P_2 \rightarrow 1s^2\,{}^1S_0$ following electron-impact excitation of Tl^{79+} ions, Phys. Rev. A **102**, 042813 (2020).

[25] A. Surzhykov, S. Fritzsche, A. Gumberidze, and T. Stöhlker, Lyman-α_1 decay in hydrogenlike ions: Interference between the $E1$ and $M2$ transition amplitudes, Phys. Rev. Lett. **88**, 153001 (2002).

[26] G. Weber, H. Bräuning, A. Surzhykov, C. Brandau, S. Fritzsche, S. Geyer, S. Hagmann, S. Hess, C. Kozhuharov, R. Märtin, N. Petridis, R. Reuschl, U. Spillmann, S. Trotsenko, D. F. A. Winters, and T. Stöhlker, Direct determination of the magnetic quadrupole contribution to the Lyman-α_1 transition in a hydrogenlike ion, Phys. Rev. Lett. **105**, 243002 (2010).

[27] Z. Hu, G. Xiong, Z. He, Z. Yang, N. Numadate, C. Huang, J. Yang, K. Yao, B. Wei, Y. Zou, C. Wu, Y. Ma, Y. Wu, X. Gao, and N. Nakamura, Giant retardation effect in electron-electron interaction, Phys. Rev. A **105**, L030801 (2022).

[28] S. Tashenov, T. Stöhlker, D. Banaś, K. Beckert, P. Beller, H. F. Beyer, F. Bosch, S. Fritzsche, A. Gumberidze, S. Hagmann, C. Kozhuharov, T. Krings, D. Liesen, F. Nolden, D. Protic, D. Sierpowski, U. Spillmann, M. Steck, and A. Surzhykov, First measurement of the linear polarization of radiative electron capture transitions, Phys. Rev. Lett. **97**, 223202 (2006).

[29] S. Tashenov, T. Bäck, R. Barday, B. Cederwall, J. Enders, A. Khaplanov, Y. Poltoratska, K.-U. Schässburger, and A. Surzhykov, Measurement of the correlation between electron spin and photon linear polarization in atomic-field bremsstrahlung, Phys. Rev. Lett. **107**, 173201 (2011).

[30] Y. Tsuzuki, S. Watanabe, S. Oishi, N. Nakamura, N. Numadate, H. Odaka, Y. Uchida, H. Yoneda, and T. Takahashi, An application of a Si/CdTe Compton camera for the polarization measurement of hard x rays from highly charged heavy ions, Rev. Sci. Instrum. **92**, 063101 (2021).

[31] M. K. Inal and J. Dubau, Theory of excitation of He-like and Li-like atomic sublevels by directive electrons: Application to x-ray line polarisation, J. Phys. B: At. Mol. Phys. **20**, 4221 (1987).

[32] M. K. Inal and J. Dubau, Polarisation of dielectronic recombination satellite lines, J. Phys. B: At. Mol. Opt. Phys. **22**, 3329 (1989).

[33] M. H. Chen and J. H. Scofield, Relativistic effects on angular distribution and polarization of dielectronic satellite lines of hydrogenlike ions, Phys. Rev. A **52**, 2057 (1995).

[34] S. Fritzsche, N. M. Kabachnik, A. Surzhykov, and T. Stöhlker, Breit interaction effects on the Kα angular distribution following the dielectronic recombination of high-Z ions, Nucl. Instrum. Methods Phys. Res. B **267**, 257 (2009).

[35] S. Fritzsche, A. Surzhykov, and T. Stöhlker, X-ray emission from highly charged ions following dielectronic recombination: Relativistic effects upon angular distributions and polarization, Phys. Scr. **T144**, 014002 (2011).

[36] P. Beiersdorfer, D. A. Vogel, K. J. Reed, V. Decaux, J. H. Scofield, K. Widmann, G. Hölzer, E. Förster, O. Wehrhan, D. W. Savin, and L. Schweikhard, Measurement and interpretation of the polarization of the x-ray line emission of heliumlike Fe XXV excited by an electron beam, Phys. Rev. A **53**, 3974 (1996).

[37] O. Matula, S. Fritzsche, F. J. Currell, and A. Surzhykov, Angular correlations in radiative cascades following resonant electron capture by highly charged ions, Phys. Rev. A **84**, 052723 (2011).

[38] M. F. Gu, The flexible atomic code, Can. J. Phys. **86**, 675 (2008).

[39] G. W. F. Drake, Spontaneous two-photon decay rates in hydrogenlike and heliumlike ions, Phys. Rev. A **34**, 2871 (1986).

[40] D. Banaś, A. Gumberidze, S. Trotsenko, A. V. Volotka, A. Surzhykov, H. F. Beyer, F. Bosch, A. Bräuning-Demian, S. Fritzsche, S. Hagmann, C. Kozhuharov, A. Kumar, X. Ma, R. Mann, P. H. Mokler, D. Sierpowski, U. Spillmann, S. Tashenov, Z. Stachura *et al.*, Two-photon energy distribution from the decay of the $2\,{}^1S_0$ state in He-like uranium, Phys. Rev. A **87**, 062510 (2013).

[41] V. V. Balashov, A. N. Grum-Grzhimailo, and N. M. Kabachnik, *Polarization and Correlation Phenomena in Atomic Collisions* (Springer, New York, 2000).

[42] S. Fritzsche, N. M. Kabachnik, and A. Surzhykov, Angular distribution of the dielectronic satellite lines from relativistic high-Z ions: Multipole-mixing effects, Phys. Rev. A **78**, 032703 (2008).

[43] C. J. Fontes, D. H. Sampson, and H. L. Zhang, Inclusion of the generalized Breit interaction in excitation of highly charged ions by electron impact, Phys. Rev. A **47**, 1009 (1993).

[44] N. Nakamura, Breit interaction effect on dielectronic recombination of heavy ions, J. Phys. B: At. Mol. Opt. Phys. **49**, 212001 (2016).

[45] M. F. Gu, D. W. Savin, and P. Beiersdorfer, Effects of electron spiralling on the anisotropy and polarization of photon emission from an electron beam ion trap, J. Phys. B: At. Mol. Opt. Phys. **32**, 5371 (1999).

[46] Z. Yang, J. Gao, W. Yan, K. Yao, J. Yang, Z. Wu, and Z. Hu, Anisotropy and polarization of x-ray line emissions in the dielectronic recombination of hydrogenlike Fe^{25+} ions, Phys. Rev. A **104**, 022809 (2021).

[47] Z. W. Wu, Z. M. He, Z. Q. Tian, C. Z. Dong, and S. Fritzsche, Angular and polarization properties of the Lyman-α_1 line $2p_{3/2} \rightarrow 1s_{1/2}$ following electron-impact excitation of hydrogenlike ions, Phys. Rev. A **105**, 062813 (2022).

[48] K. Ma, S.-X. Wang, L.-F. Zhu, Z.-M. Tang, and L.-Y. Xie, Multipole mixing effects on the angular distribution and polarization of dielectronic hypersatellite lines from highly charged helium-like ions, Phys. Lett. A **475**, 128852 (2023).

[49] Z.-M. Hu, Y.-M. Li, A. Yamazaki, and N. Nakamura, Two-photon observations of dielectronic recombination processes, Phys. Scr. **T144**, 014047 (2011).